Nanoscale

Accepted Manuscript

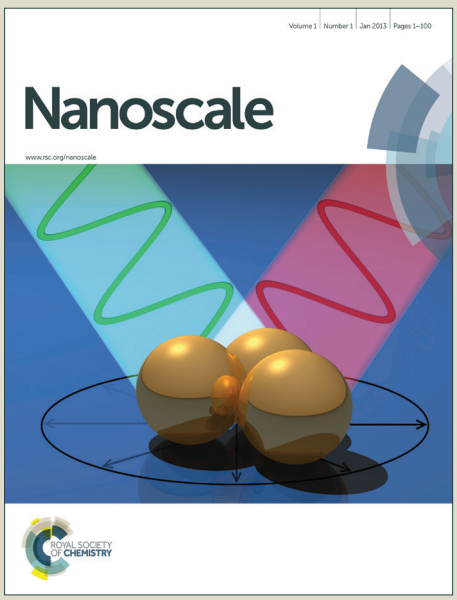

ROYAL SOCIETY OF CHEMISTRY

www.rsc.org/nanoscale

Journal Name

RSCPublishing

ARTICLE

Ultrarapid and Ultrasensitive Electrical Detection of Proteins of in Three-Dimensional Biosensor with High Capture Efficiency

Cite this: DOI: 10.1039/x0xx00000x

Received 00th January 2012,
Accepted 00th January 2012

DOI: 10.1039/x0xx00000x

www.rsc.org/

Bo-Yeong Kim[a], Il-yung Sohn[b], Doowon Lee[b], Gill Sang Han[b], Won-Il Lee[c], Hyun Suk Jung[b], Nae-Eung Lee[a,b,c,*]

Realization of a high-throughput biosensor platform with ultrarapid detection of biomolecular interactions and ultralow limit of detection in the femtomolar (fM) range or below has been retarded due to sluggish binding kinetics caused by the scarcity of probe molecules on the nanostructures and/or limited mass transport. Here, as a new method for highly efficient capture of biomolecules at extremely low concentration, we tested a three-dimensional (3D) platform of bioelectronic field-effect transistors (bio-FETs) with vertically aligned and highly dense one-dimensional (1D) ZnO nanorods (NRs) as a sensing surface capped by an ultrathin TiO_2 layer for improved electrolytic stability on a chemical-vapor-deposited graphene (Gr) channel. The ultrarapid detection capability with a very fast response time (~ 1min) at the fM level of proteins in the proposed 3D bio-FET is primarily attributed to the fast binding kinetics of the probe-target proteins due to a small diffusion length of the target molecules to reach the sensor surface and the substantial number of probe molecules available on the largely increased surface area of the vertical ZnO NRs. This new 3D electrical biosensor platform can be easily extended to other electrochemical nanobiosensors and has great potential for practical applications in miniaturized biosensor integrated systems.

Introduction

Extensive research efforts have sought to develop fast, highly sensitive, and miniaturized biosensors for point-of-care diagnostics[1-5]. In particular, the use of nanostructure materials in electrochemical[6-16] and gravimetric biosensors[17] has attracted great attention due to possibility of obtaining high sensitivity, low limit of detection (LOD), and real-time and label-free detection, because nanostructure materials show extremely high sensitivity to bimolecular interactions. The detection of extremely dilute target molecules at the femtomolar (fM) level or below is of great interest for clinical diagnostics of diseases with low concentration biomarkers and for the detection of secreted biomolecules from a single cell.[14, 17-19] However, development of these high-throughput nanobiosensor platforms with ultralow LODs at the fM level or below and with high sensitivity and ultrarapid detection (within a minute) of biomolecular interactions has not been achieved because the binding kinetics of probe-target molecules are limited by the small number of probe molecules on the small surface of the nanostructures and/or limited mass transport to the sensor's surface.[1] To achieve ultrarapid and ultrasensitive detection in the minute range at target concentrations in the fM level, it is essential to develop engineered probe molecules with high affinity and selectivity, to increase the immobilized density of probe molecules in a given sensor area, and/or to optimize sensor geometry to increase mass transport for fast binding kinetics of target molecules with probe molecules.[1, 17, 20-22]

The binding kinetics of the probes and target molecules on nanosensors or microsensors in lateral flow systems is generally described by the Damköhler number, D_a, which is a ratio of reactive to diffusive flux.[1, 17] The Damköhler number can be expressed as $D_a = k_{on} b_m A_s/(J_D/C_o)$, where k_{on} is the rate of association, b_m is the surface density of probe molecules on the sensor surface, A_s is the surface area of the sensor (here, ZnO nanorods (NRs)), J_D is the collection rate of target molecules reaching the sensor surface, and C_o is the concentration of target molecules.[1, 17] For $D_a \gg 1$, the binding kinetics are entirely mass-transport limited, while for $D_a \ll 1$, the kinetics of capture become reaction limited. Experimentally, one-dimensional (1D) bioelectronic field-effect transistors (bio-FETs) based on a single Si nanowire (NW) showed ultrasensitive detection of proteins and deoxyribonucleic acids (DNAs) down to concentrations in the fM range and with response times of several tens of minutes.[23-25] However, other

experiments and numerical considerations on the protein binding kinetics on Si NW bio-FETs showed contradictory results with response times of several tens of minutes at pM levels or above.[17, 20, 26, 27] For example, numerical simulations on 1D NW nanosensors in the microfluidic channel indicated that the binding kinetics are reaction limited.[1] It may take several days for one target molecule to be attached to the single NW surface at the fM level because binding events of target and probe molecules rarely happen at extremely low C_o due to the scarcity of probe molecules on the small area of Si NW giving a very small $b_m \cdot A_s$ value.[1] A lack of saturation in the sensing signal in 1D nanobiosensors can limit the LOD during detection of protein-protein interactions. To expedite the detection speed with fast binding kinetics at extremely low C_o, therefore, it is important to develop new approaches to simultaneously increase the $b_m \cdot A_s$ value and the diffusion flux, J_D simultaneously.[20]

Bio-FETs based on a two-dimensional (2D) nanomaterial channel with a microscale sensing area are capable of achieving ultrarapid detection of biomolecular interactions due to their relatively larger $b_m \cdot A_s$ values; they have a larger number of probe molecules on the sensing channel. In this sense, 2D bio-FETs based on graphene (Gr),[9, 11, 12, 28, 29] reduced graphene oxide (rGO)[30, 31] and MoS_2 [32, 33] have potential as biosensors for the rapid detection of protein and DNA interactions. For example, a 2D bio-FET based on a large area rGO channel showed a response time of about 12 minutes for the detection of the prostate specific antigen/1-antichymotrypsin (PSA-ACT) complex, a protein biomarker for prostate cancer, at the 1 fM level.[30]

Even though there is still room for improvement in the detection speed of extremely dilute target molecules, there have been no such efforts for development of bio-FETs having the capability of ultrarapid detection with response time near one minute. As a new method, three-dimensional (3D) channel structures with vertical, highly dense 1D NWs or NRs on a microscale channel in bio-FETs are interesting because the surface area of the channels can be increased dramatically for functionalization of a large number of probe molecules in a given device area, and the diffusion distance of probe molecules to reach the probe-functionalized surface of the vertical 1D nanostructures can be reduced to the nanoscale level for effective mass transport. However, to our knowledge, there have been no such studies on immunosensing using bio-FETs with 3D channel structures.

Herein, we demonstrate 3D bio-FETs with vertical, highly dense ZnO NRs sensing materials on chemical vapor-deposited (CVD) Gr channel which is an excellent substrate for directional growth of ZnO NRs and their ambipolar characteristics enable one to extract the sensing parameters more clearly. Furthermore, the conductance of the CVD Gr channel can be easily modulated by the electrical responses from biomolecular interactions on the surface of the ZnO NRs because of the high electrical coupling between Gr and ZnO NRs.[34] A 3D bio-FET with vertically grown ZnO NRs on a Gr channel was successfully fabricated with ambipolar characteristics. The fabricated 3D bio-FETs were used to detect the target analytes of the PSA-ACT complex. We obtained a sensitivity of ~8 mV/dec from the charge neutrality point (CNP), a dynamic range of 10^7, a LOD of 100 fg/ml (~1 fM), and a detection time of 64 s at a target concentration at the fM level. The 3D bio-FET showed significant improvements in sensitivity, dynamic range, and response time compared to other 1D or 2D bio-FETs.

Results and discussion

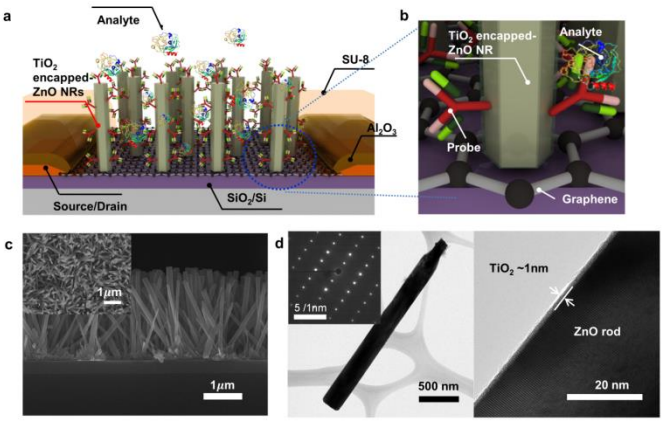

Figure 1. (a) Schematic illustration of a 3D channel FET biosensor. The ZnO NRs were vertically grown on the Gr channel area. The source/drain electrodes are electrically isolated from the analyte solution by passivation of a thin Al_2O_3 layer and SU-8 pattern. (b) Schematic showing the immobilization of antibody probe molecules on the surface of TiO_2-encapped ZnO NR. (c) Cross-sectional FE-SEM image of ZnO NRs grown on CVD Gr (Inset: top view FE-SEM image). ZnO NRs approximately 2.5 μm in length with a hexagonal shape were grown on Gr using a solution growth method. (d) Micrograph of a TiO_2-encapped ZnO NR with the selected area diffraction pattern as an inset (left) and high-resolution image of the ultrathin TiO_2 layer capping the ZnO NR (right) obtained by transmission electron microscopy.

A schematic illustration of a 3D channel bio-FET with vertically grown ZnO NRs on the CVD Gr of the SiO_2/Si wafer and biofunctionalization with PSA-ACT complex probe molecules is illustrated in Figures 1a and 1b. The channel length between the source and drain electrodes of the 3D channel FET was set at 300 μm, and the channel width was 6000 μm. Details of fabrication process of 3D bio-FET (Figure S1) are explained in experimental section. The single layer graphene (SLG) on the SiO_2/Si wafer as a transport channel was transferred using a gold (Au) transfer method previously developed by our group, which provided an ultraclean surface for further surface functionalization and high electrical performance.[29, 35] Growth of ZnO NRs on the Gr channel was achieved using a solution growth method.[36-40] Details of SLG synthesis and transfer process are provided in experimental section. Cross-sectional- and top-view images of the grown

ZnO NRs obtained by field-emission scanning electron microscopy (FE-SEM) indicated the average height (H) and diameter of ZnO NRs at ~2.5 μm and ~170 nm, respectively (Figure 1c). Assuming a uniform distribution of ZnO NRs on the channel area, the ratio of the total sensing surface area of ZnO NRs (A_s) to the device channel area (A_c), A_s/A_c, was estimated to be ~23, which suggests a dramatic increase in the sensing area of 3D ZnO NRs compared to that of 2D Gr. Details of characterization of the CVD Gr and ZnO NRs are described in the Figure S2. A further important feature of this fabrication method is the passivation of the source and drain electrodes using a photo-patternable SU-8 epoxy from the electrolyte to minimize the leakage current between the electrolyte and the electrodes and attachment of the probe molecules on the source-drain electrodes (see the details in experimental section). Due to the instability of ZnO NRs in aqueous environments[41], the surface of ZnO NRs was also capped by an ultrathin TiO_2 layer (~1 nm) [42] *via* atomic layer deposition (ALD) (Figure S3). The image of a TiO_2-encappd ZnO NR obtained by high-resolution transmission electron microscopy (Figure 1d) confirmed the ultrathin TiO_2 layer on the ZnO NR surface.

To understand the fundamental characteristics of solution-gated 3D channel FETs, their responses to solutions with different ionic concentrations were investigated. The transfer characteristics, source-drain current (I_{DS}) versus the gate bias voltage (V_G), of 3D channel FETs and Gr FETs measured in sodium phosphate buffer solutions with various ionic concentrations at a fixed pH 7.4 are shown in Figures S4a and S4b, respectively. Interestingly, the 3D channel FET showed excellent ambipolar transfer characteristics similar to that of Gr FET. For both 3D and 2D Gr channel FETs, the transfer curve shifted to a more negative voltage when the ionic concentration of the buffer solutions was increased, and changes in the conductivity and CNP occurred at same time.[43] The electrical double layer (EDL) thickness decreased when the ionic concentration increased, which accompanied an increase of EDL capacitance value resulting in reduced surface potential and, in turn, a shift of charge neutrality point (CNP) in the negative direction.[44] Similar behaviors were reported for electrolyte-gated SLG FETs, which were explained by electrostatic gating effects.[43, 45-47] The sensitivity of the 3D channel FET to ionic concentration was notably higher than that of Gr FET (Figure S4c). Increased responsivity of the 3D channel FET to ionic strength is attributed to the increased surface area of the 3D channel due to the high density, high aspect-ratio ZnO NRs on the Gr layer.

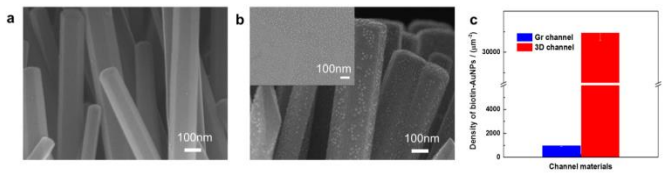

Figure 2. The FE-SEM images were observed to confirm the binding of gold nanoparticles conjugated with biotin (biotin-AuNPs) and streptavidin functionalized on the TiO_2 surface: (a) before and (b) after O_2 plasma treatment of TiO_2/ZnO NRs, respectively. The inset in Figure 4c was obtained after binding of biotin-AuNPs with streptavidin functionalized on the Gr surface using PBSE linker molecules. (c) The density of biotin-AuNPs biomolecules of 3D and Gr channel FETs at a channel surface area of 1 μm^2. The density of biotin-AuNPs indirectly reflects the density at which probe biomolecules are immobilized on the sensing channels.

In bio-FETs used for immunosensing, having a high density of probe proteins on the channel surface is critical to enhance sensitivity, LOD, and dynamic range. Details of the immobilization procedure are described in the Figure S5. To confirm the effective immobilization of the probe proteins on the surface of TiO_2-encapped ZnO NRs at a high density before and after oxygen plasma treatments[48,] biotin-streptavidin complexes were used as a test of protein interactions. For this purpose, streptavidin was first immobilized as a probe protein on TiO_2-encapped ZnO NRs using primary amine group in protein, and the ZnO NRs were incubated with the biotin-AuNP solution for 30 min. After binding of streptavidin molecules and biotin-AuNPs, the TiO_2-encapped ZnO NRs with and without plasma treatments were characterized by FE-SEM (Figures 2a and 2b). Clearly, the density of biotin-AuNPs is much higher after (Figure 2b) oxygen plasma treatment than before (Figure 2a), due to the increased density of streptavidin probe molecules immobilized onto the plasma-treated surface. The surface density of AuNPs on TiO_2-capped ZnO NRs was ~$10^3/\mu m^2$, which is comparable to that on the Gr (inset in Figure 2b). The calculated density of AuNPs on the surface of the 3D channel for a given channel area of 1 μm^2 was higher than that on the surface of the Gr channel by a factor of 32 (Figure 2c). After efficient functionalization of the TiO_2-encapped ZnO NRs by the streptavidin protein was confirmed, immunosensing of prostate specific antigen/1-antichymotrypsin (PSA-ACT) complex antigen (Ag) as an analyte and PSA-ACT antibody (Ab) as a probe was carried out. The PSA-ACT complex is widely used as a biomarker for the diagnosis of prostate cancer, because PSA is generated from prostatic tissue. Typically, men without prostate cancer have PSA levels below 4.0 ng/ml, while men with prostate cancer have PSA concentrations above 20.0 ng/ml.[49] Early diagnosis is the best way to reduce patient mortality, and quantitative monitoring of PSA is important to patients. Detection of PSA-ACT complex antigen (PSA-ACT complex Ag) was carried out in by static and kinetic measurements. The PSA-ACT Ab was immobilized in the same way as shown in Figure S5. The transfer characteristics before and after immobilizing PSA-ACT Ab probe molecules on 3D and 2D channel FETs were shown in Figure S6a and S6b, respectively. The larger decreases in the I_{DS} and CNP of 3D channel FET were observed compared to those of 2D channel FET. Those results obtained from the 3D channel FET (Figure 3) may explain the high sensitivity and

wide dynamic range that are attributed to the largely increased density of immobilized Ab probe molecules over the same channel area. Since the charges of proteins are minimally detected by charge screening effects outside the Debye screening length, the analyte solution was prepared by controlling the amount of PSA-ACT complex Ag in the diluted phosphate buffered saline (PBS) solution.[30, 31, 50] Accordingly, we carried out immunosensing measurements by diluting analyte molecules in a 1 μM PBS solution, pH of 7.4, with a Debye length of ~70 nm, which is larger than that of the combined PSA-ACT Ab-Ag (~15 nm). All measurements were carried out at a V_G of 1 V to avoid electrolysis by high gate voltage sweep and after blocking using ethanolamine at 100 mM to prevent interactions between unreacted -CHO groups of glutaraldehyde and the PSA-ACT complex Ag.

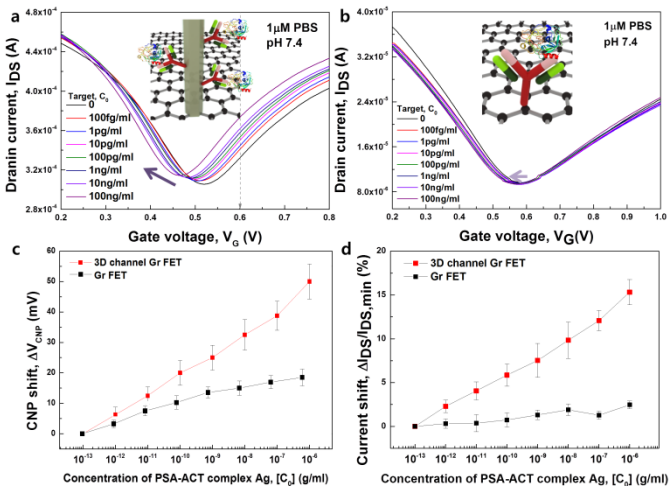

Figure 3. Transfer characteristics before and after adding different concentrations of PSA-ACT complex Ag molecules from 100 fg/ml to 100 ng/ml for (a) 3D channel Gr FETs (TiO_2-encapped ZnO NRs/Gr) and (b) Gr FETs. (c) The shift in charge neutrality point (CNP) as a function of analyte concentration, $\boldsymbol{C_o}$. (d) Drain current (I_{DS}) of 3D and Gr channel FETs as a function of analyte concentration, $\boldsymbol{C_o}$. The CNP was negatively shifted upon increasing the concentration of PSA-ACT complex Ag. The increased I_{DS} and the negative CNP shift ($\boldsymbol{\Delta V_{CNP}}$) with increasing the concentration of PSA-ACT complex Ag molecules were obtained from the transfer curves like ones in Figures (a) and (b) at a gate voltage (V_G) of 0.6 V in the linear region. The data in (c) and (d) were averaging the values obtained from five bio-FETs.

The transfer characteristics of 3D and 2D bio-FETs with the analyte concentration, C_o, of the PSA-ACT complex Ag from 100 fg/ml (1.1 fM) to 100 ng/ml (1.1 nM) at V_{DS} = 0.1 V, respectively, are shown in Figures 3a and 3b. The transfer curves of both solution-gated bio-FETs were obtained over 10 min while simultaneously adding the analyte solution. For both 3D and 2D bio-FETs, the CNP in the transfer curves (V_{CNP}) shifted to negative V_G; the current gradually increased with the increase of the PSA-ACT complex Ag concentration. However, the transfer characteristics of the two solution-gated bio-FETs demonstrated a clear difference in the degree of shift of CNP. The V_{CNP} in both FETs was quantified and plotted as a function of the PSA-ACT complex Ag concentration (Figure 3c). Shift in the CNP (ΔV_{CNP}) can be used as a sensitivity parameter due to its superior linearity and large dynamic range of 10^7. The use of ZnO NRs on the Gr channel significantly increased the V_{CNP} from ~2.3 mV/dec in the Gr FET to ~8 mV/dec in the 3D FET, indicating that the transduction of biomolecular interactions into the electrical conductance change of the Gr channel intensified using the vertical ZnO NRs. The CNP shift is suggested to occur via an electrostatic gating effect, as was previously described in CNT or Si NW bio-FETs.[51] If electrostatic gating effects occur, the CNP would be shifted in the positive direction, as the negative charges of bound PSA-ACT Ag molecules increase at pH 7.4. The PSA-ACT complex Ag is negatively charged above its isoelectric point of 6.8. Negative shifts in CNP with the concentration of target Ag molecules (Figure 3a) suggest electron doping, which contrasts with hole doping by the electrostatic gating effect. The same phenomenon was observed with the Gr FET (Figures 3b and 3c) and has also been reported for rGO FET[30, 31] and CVD Gr FET[28, 29, 52] during protein or DNA interactions. Electron doping in the 3D channel FET is ascribed to the transfer of electrons through the ZnO NRs from biomolecules. Considering the difficulty of direct transfer of biomolecular charges to Gr through ZnO NRs; however, the effects of biomolecular charges on the Fermi level of the n-type ZnO NRs are plausible, because the electron affinities of ZnO NRs (~ -4.4 eV) and Gr (~ -4.3 eV) are nearly equal. Transfer of electrons from ZnO NRs to the Gr channel increases the Fermi level of Gr, which results in a negative CNP shift. A detailed understanding of the sensing mechanism requires further theoretical and experimental studies. Moreover, the 3D channel FET immobilized with PSA-ACT Ab molecules did not show notable tendencies in the shifts of CNP and I_{DS} upon adding carcinoembryonic antigen (CEA) solution with the wide range of concentration ranging from 100 fg/ml to 100 ng/ml during the reaction time of 10 min (Figure S7). The results indicate that PSA-ACT Ab-Ag binding in the 3D channel FET was specific.

The changed I_{DS} values were plotted against increasing PSA-ACT complex Ag concentrations for the two types of FETs (Figure 3d). The I_{DS} change is obtained from the linear region in the transfer curves at V_G = 0.6 V. The I_{DS} modulation data also show good linearity in the 3D FET compared with that in the 2D FET. Therefore, modulation of I_{DS} can also be used as a sensitivity factor during immunosensing. The modulation of I_{DS} ($I_{DS}/I_{DS,min}$) in the 3D FET (~2.18%/dec) was larger than that in the 2D FET (~0.3%/dec) upon increasing the PSA-ACT complex protein Ag. These results support the potential of our developed 3D FET for immunosensing.

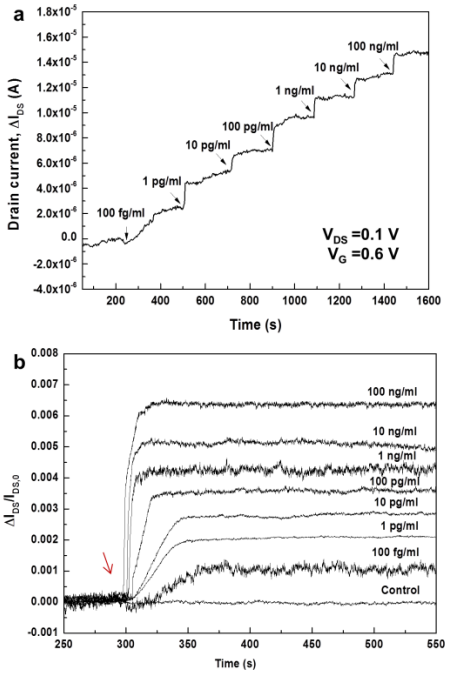

Figure 4. (a) Responses of 3D channel FET upon adding the analyte solutions in different concentrations with a step-wise increase. (b) Time-dependent kinetic responses of 3D channel FETs upon adding the analyte solutions at different concentrations. Each response curve was obtained from different devices. The arrow indicates the time when the antigen solutions are added.

Kinetic measurements were employed to detect PSA-ACT complex Ag by stepwise addition of the Ag molecules. Measurements were carried out at fixed V_{DS} = 0.1 and V_G = 0.6 V. There were significant changes in the I_{DS} of the 3D bio-FET upon adding analyte solutions in low concentration ranges (Figure 4a), but no significant changes were observed in the I_{DS} of Gr channel FET (Figure S8). The I_{DS} in the 3D bio-FET increased in a stepwise fashion when analyte solutions with different concentrations were added. When the same volume of PBS solution without analytes into the PDMS well on the 3D FET was added, the I_{DS} was not modulated (Figure S9). Furthermore, the 3D channel FET was applied to detect the target molecules of PSA-ACT Ag in diluted human serum (0.1%) and the measured data for the concentration of 100 fg/ml, 100 pg/ml and 100 ng/ml of PSA-ACT complex in human serum are shown in Figure S10a. The results in Figure S10a indicate that the sensor signals in diluted human serum are similar to those of the specific PSA-ACT Ab-Ag binding reaction in diluted PBS solution. However, the sensor responses for the minimum 100 fg/ml concentration of PSA-ACT complex Ag in 1.0 and 10% diluted human serums are negligible (Figure S10b), which is attributed to the charge screening of PSA-ACT Ag molecules in the less diluted human serums having larger ionic strength and, in turn, shorter Debye screening length.

Time-dependent responses of bio-FETs upon adding each target solution with different Ag concentrations from 100 fg/ml to 100 ng/ml were measured and plotted by normalizing the responses as $\Delta I_{DS}/I_{DS,0}$ for each concentration (Figure 4b). As the Ag target concentration increased, saturation occurred more rapidly; the increase in the response time matched well with the results of the static measurements at V_G = 0.6 V. At concentrations of 100 fg/ml and 100 pg/ml, for example, the normalized signal was saturated after 64 and 44 s, respectively. Based on the Langmuir model, [53, 54] an association constant, K_A, of ~16 pM^{-1} and a k_{on} of ~10^6 $M^{-1}\cdot s^{-1}$ were obtained (see Figure S11). This value is different from the reported values of, for example, ~ 0.9 nM^{-1} for immunoreactions of PSA mAb and anti-PSA from surface plasmon resonance biosensor[55] and 0.4 pM^{-1} for immunoreactions of PSA mAb and anti-PSA in SiNW bio-FET.[56] The K_A value in this work was also smaller than that in the 2D rGO bio-FET (~4.2 nM^{-1}) reported previously by our group.[30] Even though the reason for this discrepancy for planar 2D and vertically nanostructured 3D surfaces is not clearly understood, it is presumed that the observed discrepancy is possibly attributed to differences in the density, orientation or binding states of immobilized Ab biomolecules on planar 2D and vertical 1D surfaces resulting in the different binding reactions at equilibrium. Better understanding of the discrepancy may require a further study on the quantitative kinetic analysis in microfluidic systems similarly to the approach by Duan et al.[20]

In the well containing bulk target solutions with a relatively large volume (400 µl), the mass transport of target molecules occurs by diffusion. When considering the diffusivity D of proteins in solution is the order of 1~10 $\mu m^2/s$,[1] the bulk diffusion time of the target proteins towards the ZnO NRs is in the order of 10^1~10^2 mins. Indeed, the diffusion time on the 2D rGO channel bio-FET was in the order of tens of min.[30] On the other hand, observed ultrafast response time in the 3D channel FET is presumably attributed to fast binding of the Ag molecules in between ZnO NRs as well as in the vicinity of vertical 1D ZnO NRs. Since the time scale of mass transport of target molecules in between ZnO NRs towards the NR surface is in the order of 10^{-5} s considering an average distance between NRs of 50-100 nm, the diffusion of target molecules from the bulk solution only near the top surface of ZnO NRs vertically towards the region of ZnO NRs can be considered. The time scale of vertical mass transport to the bottom of the ZnO NRs was approximated in the order of a few seconds after considering the height of the ZnO NRs, H, of ~2.5 µm. In this situation, the collection rate of target molecules towards the ZnO NRs was approximated by $J_D = A_c D C_o / H$, where the target concentrations at the top and bottom of the ZnO NRs were assumed to be C_o and zero by neglecting depletion of target molecules above ZnO NRs. Then, the Damköhler number is given by $D_a = k_{on} b_m (A_s/A_c)/(D/H)$. Due to difficulty of direct measurement of b_m for the PSA Ab-Ag interactions on the ZnO NRs, the surface density of biotin-Au NPs from streptavidin-biotin interactions, ~$10^3/\mu m^2$, was used as the b_m value on the ZnO sensing surface. This value was lower than

the surface density of the PSA Ab probes on rGO, which were indirectly estimated at ~$2\times10^5/\mu m^2$.[30] The D_a value was estimated as ~11, which indicates a mass-transport limited regime during Ab-Ag interactions in the 3D channel. We presume that, while the mass transport from the bulk solution towards the ZnO NRs determines overall binding kinetics, added Ag molecules would be easily captured because of the large number of probe molecules (a large $b_m \cdot A_s$ value) and the short distance in between vertical ZnO NRs and, as a result, faster binding kinetics would lead to a faster electrical response. The range of detection time observed in the present immunosensing method, close to 1 min at fM level, is much shorter than the several tens of minutes to hours typically observed for 2D rGO[30] or 1D NW[20] biosensors.

As an alternative reason for ultrafast response, some charged species near the ZnO NR surface in proximity under the electrical operation of the device might be related to the fast binding kinetics of Ag molecules because negatively charged Ag molecules or other charged particles can be drifted. To investigate the effect of gate electric field on binding kinetics, detection of immunoreactions was measured in the 3D channel FET under no gate biasing (V_G = 0V). The reaction time of PSA-ACT complex at 100 fg/ml concentration under no gate biasing was ~ 70 s (Figure S12) similarly to that of 3D FET under positive gate biasing, which presumably indicates that the drift of charged particles by gate biasing negligibly affects the binding kinetics. The feature of fast response time in 3D bio-FET could be very important for applications of miniaturized nanobiosensors in diagnostic technology utilizing microfluidic channels where the binding kinetics are limited due to the depletion of target molecules near the 2D sensing surface.[1] Further verification of binding kinetics in microfluidics with mass transport of simultaneous convection and diffusion is needed to elucidate the optimal sensor mechanism and design. The measurement of immunoreactions in the 3D bio-FET indicates the clear advantages of ultrahigh sensitivity, large dynamic range, and ultrafast response time in the field of immunosensing.

Conclusions

Here, we presented a new sensing platform for a 3D channel bio-FET based on nanostructured materials. We successfully developed a bio-FET with a 3D channel composed of TiO_2-encapped ZnO NRs vertically grown on CVD Gr for a label-free, ultrasensitive, and ultrarapid electrical biosensor for immunosensing. An ultrathin layer of TiO_2 solved the problem of the chemical instability of ZnO NRs in the electrolyte. The use of a 3D channel dramatically increased the number of probe molecules immobilized on the dense, vertical TiO_2-encapped ZnO NRs in a given channel area compared to that on the 2D Gr channel. Increased probe molecules in a given channel area resulted in a significant improvement in static measurement sensitivity. The results from the 3D channel bio-FET also indicated an extremely large dynamic range of 10^7 and a sensitivity of 8 mV/dec from CNP shifts. The large sensing surface area and shorter distance between vertically grown ZnO NRs facilitated the binding kinetics of analyte-target protein molecules resulting in a fast response time of ~64 s at an analyte concentration of 100 fg/ml (~1 fM). More researches including reusability of the 3D bio-FET sensor and detailed kinetic analysis need to be performed for further advancement of 3D channel bio-FET in near future. The proposed 3D biosensing platform can be easily extended to the detection of various biomolecules other than proteins and various electrochemical detection schemes including voltammetry, amperometry or impedimetry. Therefore, the newly developed 3D electrochemical 3D bio-FET platform based on nanostructured materials has great potential to be applied to a variety of biosensing systems including disease diagnostics, environmental monitoring, and food safety.

Experimental

Graphene synthesis: SLG was synthesized using the CVD method on copper foil (0.025mm, Alfa Aesar). Copper foil was cleaned with acetic acid, placed in the middle of a quartz tube furnace, and heated at 1000˚C under a H_2 gas flow of 40 sccm for 20 min. Subsequently, 20 sccm of CH_4 gas was flowed into the tube in order to grow Gr followed by a mixture of H_2 and CH_4 gasses at a 2:1 ratio and a pressure of 300 mTorr for 20 min. The heated copper foil was cooled to room temperature under an H_2 atmosphere.

Graphene transfer: Synthesized SLG was transferred using a gold layer method that can reduce defects and give a very clean Gr surface. A 25-nm gold layer was deposited on Gr grown on copper foil at a deposition rate of 0.1Å/s using a thermal evaporator. Gold/graphene was separated from the copper foil with a $FeCl_3$ copper etchant for 2 h (Alfa Aesar) and then subsequently transferred to an acetone/ethanol-cleaned SiO_2 (300 nm)/Si substrate. The sample was cleaned with three rinses of DI water over a 4 h period. After cleaning, the gold/graphene/SiO_2 was naturally dried and annealed to remove water molecules from the interface graphene between SiO_2 at 180˚C for 1 h. The gold layer was then wet etched using a gold etchant (Alfa Aesar) consisting of KI/I_2 and DI water.

Fabrication process of 3D channel FET: A schematic illustration of the device is shown in Figure S1. Source and drain electrodes of Cr (5 nm) and Au (45 nm) were deposited onto patterned Gr using a shadow mask via an e-beam evaporator (Figure S1a and S1b). The entire device was covered with an Al_2O_3 layer of 10 nm as a buffer via ALD (Figure S1c), and the active area was patterned for active area opening through positive PR photolithography. Using phosphoric acid (~85 wt%, Sigma-Aldrich), the Al_2O_3 the Gr surface was etched at 45˚C for 90 s and immediately washed with DI water (Figure S1d). The Al_2O_3 layer was used as a buffer layer to prevent direct contact with various polymers during the photolithographic process and to reduce the leakage current of the device in an aqueous environment. Acetone at 40˚C for 30 min was used to remove positive PR (Figure S1e).

ZnO NRs growth and capping by TiO_2: The solution growth method has been widely used to grow ZnO NRs because of its

low temperature growth, size control, and low cost. A dispersion solution of 10 wt% amine-modified ZnO (NPs) in water was dropped onto the graphene surface as a seed and allowed to dry for 10 min (Figure S1f). Subsequently, ZnO NPs were washed using DI water and were immersed in a mixture of hexamethylenetetramine (25 mM, HMTA, $C_6H_{12}N_4$) and zinc nitrate hexahydrate (25 mM, $Zn(NO_3)_2 \cdot 6H_2O$) in water at 90˚C for 3 h. Grown ZnO NRs were rinsed with DI water and heated at 200˚C for 1 h (Figure S1g). The ZnO NRs grown on Gr as an active layer were capped with an ultrathin 1-nm TiO_2 layer using ALD.

FET encapsulation: All areas except for the channel and electrode pad (contact region for probing) of the 3D channel and Gr FETs were encapsulated using SU-8 negative PR as follows: 1) the device was coated with SU-8 using a spin coater at an optimized spinning speed and time, 2) the fully coated SU-8 device was soft-baked at 95°C for 3 min, 3) SU-8 was exposed to UV light to make the encapsulation pattern, 4) the exposed device was baked once more at 95°C for 2 min (post exposure bake), and 5) a development process was carried out in SU-8 developer for 90 s (Figure S1h). To contain physiological solution, a PDMS well (diameter of 8 mm) was attached onto the device (Figure S1i).

Functionalization of probe biomolecules:
1) 3D channel FET: To produce hydroxyl groups on the surface of the 3D channel, oxygen plasma treatment was carried out in a microwave plasma reactor. ATPES of 2.5% in ethanol was poured on the channel region at room temperature (RT) for 2 h; it was subsequently rinsed with ethanol and dried using nitrogen gas. To activate amine group-terminated APTES, the device was heated at 150°C for 20 min. Activated amine groups were reacted with 2.5% GA in a PBS solution at RT for 2 h, and the device was washed using PBS and DI water in sequence. To immobilize streptavidin (Sigma-Aldrich) or PSA-ACT complex Ab molecules (Fitzgerald) onto the surface of the 3D channel, the device was incubated with 100 μl of probe (100 μl/ml) in PBS overnight. After incubation, the channel region was rinsed with PBS.
2) Gr channel FET: The Gr surface was treated with 1-pyrenebutanoic acid and 10 mM succinimidyl ester (PBSE) in dimethylformamide (DMF) at RT for 2 h in a dark environment. After treatment, the sample was washed to remove unstacked PBSE molecules using DMF and DI water. Immobilization of probe molecules utilized the same process as the 3D channel FET.

Measurements: Functionalized 3D and Gr channel FETs were used to detect PSA-ACT complex Ag molecules (Fitzgerald). The binding of functionalized streptavidin with biotin-grafted gold nanoparticles (biotin-AuNPs) (Cytodiagnostics) was confirmed by addition of PBS containing 100 nM biotin-AuNPs. For electrical detection of immunoreactions, the 3D and Gr channel FETs with PDMS were placed on the sample holder with the probe tips. During measurements, PBS solutions with different concentrations of PSA-ACT complex Ag molecules (Fitzgerald) were added into the PDMS well, and transfer characteristics were obtained using a semiconductor parameter analyzer (HP4145B).

Acknowledgements

This research was supported by the Basic Science Research Program (2013R1A2A1A01015232) through the National Research Foundation (NRF) funded by the Ministry of Science, ICT, & Future Planning, South Korea.

Notes and references

[a]SKKU Advanced Institute of Nanotechnology (SAINT), Sungkyunkwan University, Suwon, Gyeonggi-do 440-746, South Korea, [b]Department of Advanced Materials Science & Engineering, Sungkyunkwan University, Suwon, Gyeonggi-do 440-746, South Korea, [c]Samsung Advanced Institute for Health Sciences and Technology (SAIHST), Sungkyunkwan University, Suwon, Gyeonggi-do 440-746, South Korea
*_E-mail_: nelee@skku.edu

Electronic Supplementary Information (ESI) available: Ultrarapid and Ultrasensitive Electrical Detection of Proteins of in Three-Dimensional Biosensor with High Capture Efficiency. See DOI: 10.1039/b000000x/

1 Squires T.M., Messinger R.J., Manalis S.R., *Nat. Biotechnol.*, *2008*, **26**, 417.
2 Yager P., Domingo G.J., Gerdes J., *Annu. Rev. Biomed. Eng.*, 2008, **10**, 107.
3 Mark D., Haeberle S., G. Roth, Stetten F. V., Zengerle R., *Chem. Soc. Rev.*, 2010, **39**, 1153.
4 Gubala V., Harris L.F., Ricco A.J., Tan M.X., Williams D.E., *Anal. Chem.*, 2012, **84**, 487.
5 Wan Y., Su Y., Zhu X., Liu G., Fan C., *Biosens. Bioelectron.*, 2013, **47**, 1.
6 Patolsky F., Timko B.P., Zheng G., Lieber C.M., *MRS Bull.*, 2007, **32**, 142.
7 Rusling J.F., Sotzing G., Papadimitrakopoulosa F., *Bioelectrochemistry*, 2009, **76**, 189.
8 Wei D., Bailey M.J.A., Andrew P., Ryhänen T., *Lab Chip*, 2009, **9**, 2123.
9 Yang W., Ratinac K.R., Ringer S.P., Thordarson P., Gooding J.J., Braet F., *Angew. Chem., Int. Ed.*, 2010, **49**, 2114
10 Feigel I.M., Vedala H., Star A., *J. Mater. Chem.*, 2011, **21**, 8940.
11 Stine R., Mulvaney S.P., Robinson J.T., Tamanaha C.R., Sheehan P.E., *Anal. Chem.*, 2012, **85**, 509.
12 Liu S., Guo X., *NPG Asia Mater.*, 2012, **4**, e23.
13 Wu S., He Q., Tan C., Wang Y., Zhang H., *Small*, 2013, **9**, 1160.
14 Li B.-R., Chen C.-C., Kumar U.R., Chen Y.-T., *Analyst*, 2014, **139**, 1589.
15 Yan F., Zhang M., Li J., *Adv. Healthcare Mater.*, 2014, **3**, 313.

16 Zhan B., Li C., Yang J., Jenkins G., Huang W., Dong X., *Small*, 2014, **10**, 4042.
17 Arlett J.L., Myers E.B., Roukes M.L., *Nat. Nanotechnol.*, 2011, **6**, 203.
18 Patolsky F., Timko B.P., Yu G., Fang Y., Greytak A.B., Zheng G., Lieber C.M., *Science*, 2006, **313**, 1100.
19 Chen K.-I., Li B.-R., Chen Y.-T., *Nano Today*, 2011, **6**, 131.
20 Duan X., Li Y., Rajan N.K., Routenberg D.A., Modis Y., Reed M.A., *Nat. Nanotechnol.*, 2012, **7**, 401.
21 Nair P.R., Alam M.A., *Appl. Phys. Lett.*, 2006, **88**, 233120.
22 Sheehan P.E., Whitman L.J., *Nano Lett.*, 2005, **5**, 803.
23 Zheng G., Patolsky F., Cui Y., Wang W.U., Lieber C.M., *Nat. Biotechnol.*, 2005, **23**, 1294.
24 Cui Y., Wei Q., Park H., Lieber C.M., *Science*, 2001, **293**, 1289.
25 Chen R.J., Bangsaruntip S., K.A., Kam N. W. S., Shim M., Li Y., Kim W., Utz P.J., Dai H., *Proc. Natl. Acad. Sci. U. S. A.*, 2013, **100**, 4984.
26 Bunimovich Y.L., Shin Y.S., Yeo W.-S., Amori M., Kwong G., J.R., *J. Am. Chem.Soc.*, 2006, **128**, 16323.
27 Zheng G., Gao X.P.A., Lieber C.M., *Nano Lett.*, 2010, **10**, 3179.
28 Dong X., Shi Y., Huang W., Chen P., Li L.-J., *Adv. Mater.*, 2010, **22**, 1649.
29 Jung J.H., Sohn I.Y., Kim D.J., Kim B.Y., Jang M., N.E. Lee, *Carbon*, 2013, **62**, 312.
30 Kim D.-J., Sohn I.Y., Jung J.-H., Yoon O.J., Lee N.-E., Park J.-S., *Biosens. Bioelectron.*, 2013, **41**, 621.
31 Kim D.-J., Park H.-C., Sohn I.Y., Jung J.-H., Yoon O.J., Park J.-S., Yoon M.-Y., Lee N.-E., *Small*, 2013, **9**, 3352.
32 Sarkar D., Liu W., Xie X., Anselmo A.C., Mitragotri S., Banerjee K., *ACS Nano*, 2014, **8**, 3992.
33 Wang L., Wang Y., Wong J.I., Palacios T., Kong J., Yang H.Y., *Small*, 2014, **10**, 1101.
34 Dang V.Q., Kim D.-I., L. Duy T., Kim B.-Y., Hwang B.-U., Jang M., Shin K.-S., Kim S.-W., Lee N.-E., *Nanoscale*, 2014, **6**, 15144.
35 Jang M., Trung T.Q., Jung J.-H., Kim B.-Y., Lee N.-E., *Phys. Chem. Chem. Phys.*, 2014, **16**, 4098.
36 Choi W., Shin K.-S., Lee H., Choi D., Kim K., Shin H.-J., Yoon S.-M., Choi J.-Y., Kim S.-W., *Nano Res.*, 2011, **4**, 440
37 Guo M., Diao P., Cai S., *J. Solid State Chem.*, 2005, **178**, 1864-1873.
38 Hwang J.O., Lee D.H., Kim J.Y., Han T.H., Kim B.H., Park M., No K., Kim S.O., *J. Mater. Chem.*, 2011, **21**, 3432.
39 Liu B., Zeng H.C., *J. Am. Chem. Soc.*, 2003, **125**, 4430.
40 Polsongkram D., Chamninok P., Pukird S., Chow L., Lupan O., Chai G., Khallaf H., Park S., Schulte A., *Phys. B (Amsterdam, Neth.)*, 2008, **403**, 3713.
41 Zhou J., Xu N., Wang Z.L., *Adv. Mater.*, 2006, **18**, 2432.
42 Liu M., Nam C.-Y., Black C.T., Kamcev J., Zhang L., E., *J. Phys. Chem. C*, 2013, **117**, 13396.
43 Heller I., Chatoor S., Männik J., Zevenbergen M.A.G., Dekker C., Lemay S.G., *J. Am. Chem. Soc.*, 2010, **132**, 17149.
44 Uesugi E., Goto H., Eguchi R., Fujiwara A., Kubozono Y., *Sci. Rep.*, 2013, **3**, 1595.
45 Chen F., Xia J., Ferry D.K., Tao N., *Nano Lett.*, 2009, **9**, 2571.
46 Chen F., Qing Q., Xia J., Li J., Tao N., *J. Am. Chem. Soc.*, 2009, **131**, 9908.
47 Artyukhin A.B., Stadermann M., Friddle R.W., Stroeve P., Bakajin O., Noy A., *Nano Lett.*, 2006, **6**, 2080.
48 Kim W.-J., Kim S., Lee B.S., Kim A., Ah C.S., Huh C., Sung G.Y., Yun W.S., *Langmuir*, 2009, **25**, 11692.
49 Choi Y.-E., Kwak J.-W., Park J.W., *Sensors*, 2010, **10**, 428.
50 Schasfoort R.B.M., Bergveld P., Kooyman R.P.H., Greve J., *Anal. Chim. Acta*, 1990, **238**, 323.
51 Heller I., Janssens A.M., Männik J., Minot E.D., Lemay S.G., Dekker C., *Nano Lett.*, 2007, **8**, 591.
52 Chen T.Y., Loan P.T.K., Hsu C.L., Lee Y.H., Wang J. T.-W., Wei K.H., Lin C.T., Li L.J., *Biosens. Bioelectron.*, 2013, **41**, 103.
53 Halperin A., Buhot A., Zhulina E.B., *J. Phys.: Condens. Matter*, 2006, **18**, S463.
54 Lin A., Lee A.S.-Y., Lin C.-C., Lee C.-K, *Curr. Proteomics*, 2006, **3**, 271.
55 Katsamba P. S., Navratilova I., Calderon-Cacia M., Fan L., Thornton K., Zhu M., Bos T. V., Forte C., Friend D., Laird-Offringa I., Tavares G., Whatley J., Shi E., Widom A., Lindquist K. C., Klakamp S., Drake A., Bohmann D., Roell M., Rose L., Dorocke J., Roth B., Luginbuhl B., Myszka D. G., *Anal. Biochem.*, 2006, **352**, 208.
56 Cui Y., Wang W. U., Huynh L., Lieber C. M., Ultrasensitive and Selective Multiplexing Detection of Cancer Markers Using Nanowire Nanosensors.

